The accuracy of proton stopping powers achievable with a low kilo-voltage dual energy CT

Bachelor Thesis

Silja de Waal

July 5 2019

First examiner: Emiel van der Graaf
Second examiner: Peter Dendooven

Abstract

The accuracy of determining proton stopping powers with a 30/60 kV dual energy CT scan is investigated. This research was needed to check if the determination of proton stopping powers can be tested in pre-clinical research. The method how the proton stopping power can be estimated from the electron density and the effective atomic number of the tissue is explained. The best reference material was found to be CB2-30%. A correlation curve was found between the difference in Hounsfield units (obtained from the dual energy CT) and the accuracy of the relative electron density. If the data was scaled by the curve the deviation in the relative electron density was found to be 0.3% and the correctness of the effective atomic number 0.1. The influence of noise on the Hounsfield units was investigated. It did not have an increased negative effect when a lower kV was used. It was concluded that the proton stopping power can be determined with a 30/60 kV dual energy CT-scan.

Contents

1 Introduction

A large fraction of cancer patients receives radiation therapy during the course of their treatment [1]. Currently, proton therapy is a fast developing method in radiation therapy to radiate unhealthy tissue. In proton therapy high energy protons interact with human tissues, causing mutations or complete functional disruptance of cells. The amount of cell mutations is related to the proton energy transfer, which is inversely proportional to the square of the velocity of the protons. The dependence of the energy transfer on the velocity is mainly caused by the electromagnetic interactions of the protons with the atomic electrons. These interactions increase with decreasing energy. Along the track the particle will deposit its energy and so decelerate. The deceleration will increase the amount of electromagnetic interactions, causing a high energy transfer at the end of its track, this peak is called the Bragg peak [1].
The aim in proton therapy is to position the Bragg peak inside the tumour, to accomplish the highest deposited energy inside the unhealthy tissue. However, in practice it is hard to fulfill this goal, due to uncertainties in the position and size of the target volume and the location of the Bragg peak. The location of the Bragg peak is determined by proton stopping powers (PSP). The proton stopping power is defined as the energy transfer per unit length of the tissue, traversed by the proton. PSP are tissue dependent and so information is needed of all the surrounding tissues of the tumour. At the moment, PSP for proton therapy planning are based on a calibration curve between the Hounsfield units and the PSP. The Hounsfield unit scale is a measure for the radio-density [2]. This scale is used for scaling the attenuation of the x-ray beam during a CT-scan. Currently, for proton therapy planning, the Hounsfield units are taken from Single Energy Computed Tomography (SECT). During SECT a CT scan is made with one fixed voltage applied on the x-ray tube. However, there is still an uncertainty in the calculation of the stopping power and so a margin is used of 3-3.5% [3].
Since a couple of years, a new method is in development. In this method the Hounsfield units are taken from a Dual Energy CT (DECT), which uses two distinct tube voltages to obtain two different equations. From these equations the electron density and the effective atomic number of the target tissue can be extracted. If the composition of the target material is known the PSP can be calculated [3]. In this report the method is explained to obtain the composition with the use of DECT.
The verification of the PSP with DECT is planned to be used in a new facility for preclinical research. This will be available at KVI-CART in the near future. In such a facility research with small test animals is conducted and usually the voltage of the CT scanner is lowered due to their size [4]. In this report the uncertainties in the composition of high DECT (tube voltages of 90/150 kV) and low DECT (tube voltages of 30/60 kV) are compared. The lowest pair of tube voltages will be selected that still has a considerably low uncertainty for the composition of the material. At the end noise will be introduced to the Hounsfield units to study the effect on the achieved electron density and the effective atomic number.

2 Theory

2.1 Stopping powers from mass density and composition

The dose which is deposited by a charged particle to a tissue, is determined by the linear energy transfer to that tissue (LET). For energies larger than 1 MeV, the proton stopping power (S, which induces nuclear and radiative stopping) is almost equal to the LET. The proton stopping power is tissue dependent and is given by: $S = -\frac{dE}{dx}$. With relativistic quantum mechanics, the Bethe-Bloch equation can be derived [5]. The Bethe-Bloch equation describes the stopping power of charged particles due to interaction with the atomic electrons of the tissue traversed by the particle. The equation can be used together with Bragg's additivity rule to express the proton stopping power of a certain tissue. The stopping power is directly dependent on the density of the target material and so S is often scaled by the density of the tissue, to obtain the mass stopping power, given in equation 1.

$$\frac{S}{\rho} = \frac{Z}{A}\frac{K}{M_u\beta^2}\left[\ln\frac{2m_ec^2\beta^2}{I(1-\beta^2)} - \beta^2\right] \tag{1}$$

The derivation of equation 1 can be found in [5]. Here, K is a constant in eVμm^2, which can also be found in [5]. m_ec^2 is the electron rest mass in MeV. $\beta = v/c$ is the velocity of the particle relative to the velocity of light. I is the mean excitation energy of the medium in MeV. Z/A is used for the amount of protons relative to the total amount of nucleons. M_u is the molar mass constant in kg/mol and ρ is the mass density in kg/μm^2.
A tissue can be considered as a set of atoms, each atom with its own mass fraction ω_i. So the tissue dependent parameters in equation 1 (ρ_e, $\frac{Z}{A}$ and $\ln(I)$) need to be weighted over all mass fractions ω_i.

$$\rho_e = \sum_i \omega_i\rho_{e,i} = N_a\frac{\rho}{M_u}\sum_i \omega_i\frac{Z_i}{A_i} \tag{2}$$

$$\frac{Z}{A} = \sum_i \omega_i\frac{Z_i}{A_i} \tag{3}$$

$$\ln(I) = \frac{\sum_i \omega_i\frac{Z_i}{A_i}\ln I_i}{\sum_i \omega_i\frac{Z_i}{A_i}} \tag{4}$$

The stopping power of a compound can be expressed relative to the stopping power of water [3]. The ratios of S_x and $(S/\rho)_x$ over S_{H_2O} and $(S/\rho)_{H_2O}$, respectively, are shown in equations 5 and 6. The relative electron density, $\frac{\rho_{e,x}}{\rho_{H_2O}}$, of a specific compound, x, is defined as the electron density originating from compound x relative to the electron density originating from water. It can be concluded that the stopping power of a compound can be determined if the relative electron density and the effective atomic number are known.

$$\frac{S_x}{S_{H_2O}} = \frac{\rho_{e,x}}{\rho_{e,H_2O}}\frac{\left[\ln\frac{2m_ec^2\beta^2}{I_x(1-\beta^2)} - \beta^2\right]}{\left[\ln\frac{2m_ec^2\beta^2}{I_{H_2O}(1-\beta^2)} - \beta^2\right]} \tag{5}$$

$$\frac{(S/\rho)_x}{(S/\rho)_{H_2O}} = \frac{(Z/A)_x}{(Z/A)_{H_2O}}\frac{\left[\ln\frac{2m_ec^2\beta^2}{I_x(1-\beta^2)} - \beta^2\right]}{\left[\ln\frac{2m_ec^2\beta^2}{I_{H_2O}(1-\beta^2)} - \beta^2\right]} \tag{6}$$

2.2 CT Spectrum

The x-rays from an x-ray tube are produced by the interaction of high energy electrons with an anode. A schematic overview of a x-ray tube is shown in figure 1. The electrons are produced at the cathode side, where a current (1mA-1A) is flowing through a filament. In case the current is increased more electrons will be produced and so the x-ray intensity will be enhanced. Between the cathode and the anode a high voltage is generated, such that the electrons will be strongly attracted by the anode. When the electrons hit the anode, high energy photons will be produced, creating an x-ray beam. If the voltage is increased the acceleration of the electrons will become larger, resulting in a higher photon energy.
The photons are produced by the Bremsstrahlung interactions of the electrons with the anode. If an electron moves through the electron cloud of an atom, it experiences an electrostatic attraction by the nuclei. As a result the electron deviates from its originally straight line path and it will be slowed down. A schematic overview of the effect can be seen in figure 2. Due to the deceleration the kinetic energy of the electron is lowered. This change in energy results in the production of a photon, with its energy equal to the energy shift of the electron. The deflection of the electrons can be strong (black line in figure 2), resulting in a high energy photon. Or the deflection can be weak (blue line in figure) 2, resulting in a low energy photon.

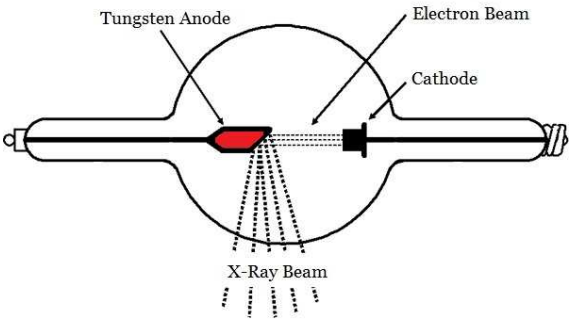

Figure 1 – X-ray tube [6]. High energy electrons generated at the cathode interact with the anode, resulting in an x-ray beam.

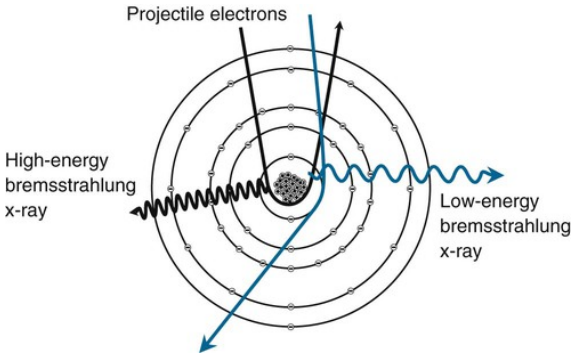

Figure 2 – Bremsstrahlung [7]. The production of photons, due to the electrostatic attraction of the electrons by the nuclei.

The dotted line in figure 3 shows the intensity of an x-ray beam produced by Bremsstrahlung as function of the photon energy. Low energy photons have a high interaction probability in the tissue due to the photoelectric effect. Consequentially low energy photons will not penetrate through the tissue and only contribute to dose to the patient and not to the formation of a CT image. To obviate this dose, a filter is used before the beam enters the tissue, such that low energy photons will not enter the tissue. Two graphs are shown for the filtered and unfiltered spectra in figure 3. In the graph, peaks occur at a specific energies, these are called the characteristic peaks. Characteristic peaks are created in the anode. Electrons are knocked out of the inner shells by the electrons coming from the cathode. A hole is created in one of the inner shells and then one of the outer electrons will fall down emitting characteristic photons with a specific energy. Due to the distinguished energy levels in the shells, several characteristic peaks may occur.

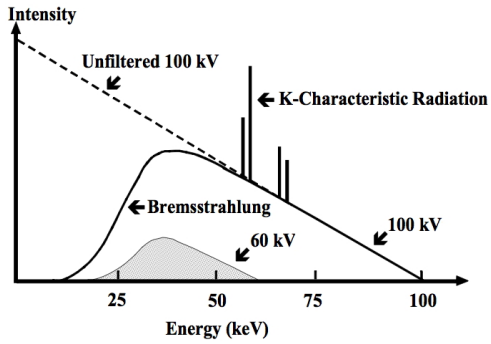

Figure 3 – The x-ray spectrum for tube voltages of 60 kV and 100 kV. On the horizontal and vertical axis the x-ray energy and intensity are given, respectively. In the figure both the filtered and the unfiltered spectra are shown by the solid and the dotted line, respectively. Also the characteristic peaks are indicated.

2.3 SpekCalc

To calculate the x-ray spectra a software program, SpekCalc, can be used. SpekCalc is designed for research and education purposes in the medical field [8]. SpekCalc is able to predict the x-ray spectrum with changeable parameters: the filters, the tube voltage and the anode angle. The angle is measured between the released photon beam and the axis perpendicular to the electron beam. More information about the geometry and the background of SpekCalc can be found in [8]. Currently, in medical imaging mostly a Siemens CT-scan is used. [9] compared the spectra from Siemens with the theoretical spectra calculated with SpekCalc. To get the best correspondence, it was found that several filtration filters were needed: 3 mm aluminum, 0.9 mm titanium and 500 mm air. The anode angle was set on 8°.

2.4 Hounsfield units

During the CT-scan the x-ray beam will be attenuated, due to interactions with the tissue. A part of the x-ray beam will pass through the tissue and the attenuation of the x-rays will be measured with a detector. Hounsfield units, HU, provide a scheme for scaling the linear attenuation coefficients in medical CT systems [10]. The Hounsfield unit is defined in equation 7 [3].

$$HU = \frac{\mu_x - \mu_{H_2O}}{\mu_{H_2O} - \mu_{air}} 1000 \approx \frac{\mu_x - \mu_{H_2O}}{\mu_{H_2O}} 1000 = \left(\frac{\mu_x}{\mu_{H_2O}} - 1 \right) 1000 = H - 1000 \tag{7}$$

In which μ_x, μ_{H_2O} and μ_{air} are the linear attenuation coefficients in tissue, water and air, respectively. The attenuation of the x-ray beam in air is much smaller compared to the attenuation in water, so μ_{air} is usually considered as negligible. To scale all the units to positive values the scaled Hounsfield unit, H, is introduced and it is defined in equation 8. So for water the Hounsfield unit is H=1000.

$$H = HU + 1000 = \left(\frac{\mu_x}{\mu_{H_2O}} \right) 1000 \tag{8}$$

2.5 Attenuation coefficient

The attenuation of the x-ray beam depends on the interactions with the sample, due to the photoelectric effect and scattering. The linear attenuation coefficient for a material x can be parameterized as [3]:

$$\mu_x(E) = \rho_{e,x}[a_{pe}Z^n f(E) + a_{sc}g(E)] \tag{9}$$

a_{pe} and a_{sc} are parameters which describe the relative strengths of the photoelectric $f(E)$ and scattering interactions $g(E)$, respectively. Both parameters are assumed to be independent of the material and the photon energy.
The average attenuation coefficient $\overline{\mu}_{x,j}$ depends on the x-ray spectrum. To take the x-ray spectrum into account the so called spectrum weighting function, w_j, for a specific tube voltage j is applied. The spectrum weighting function is given in equation 10. In this equation $S_j(E)$ is the energy distribution of the x-ray spectrum for a specific tube voltage j. $D(E)$ is the detector efficiency which is dependent on the photon energy E. To obtain the average attenuation coefficient the attenuation coefficient is weighted by w_j and it is integrated over all energies. This is expressed in equation 11. Since the photoelectric effect is dependent on the atomic number of the target material it is multiplied by Z^n. Here n is a parameter, which is found to be close to 3.3 in previous studies [3].

$$w_j(E) = \frac{S_j(E)D(E)}{\int_0^\infty S_j(E)D(E)dE} \tag{10}$$

$$\overline{\mu}_{x,j} = \rho_{e,x}\int_0^\infty w_j(E)\Big(a_{pe}Z^n f(E) + a_{sc}g(E)\Big)dE = \rho_{e,x}\Big(a_{pe}Z^n\overline{f}_j + a_{sc}\overline{g}_j\Big) \tag{11}$$

with,

$$\overline{f}_j = \int_0^\infty w_j(E)f(E)dE \quad \text{and} \quad \overline{g}_j = \int_0^\infty w_j(E)g(E)dE \tag{12}$$

2.6 Extraction of the relative electron density and the effective atomic number with the use of dual energy CT

In dual energy computed tomography two distinct tube voltages are used of typically 90 kV and 150 kV. These two different measurements provide two separate expressions for $\overline{\mu}_{x,j}$. For convention j=1 is used for a high tube voltage and j=2 for a low tube voltage. If $\frac{\overline{\mu}_{x,2}}{\overline{f}_2}$ will be subtracted from $\frac{\overline{\mu}_{x,1}}{\overline{f}_1}$ an expression for $\rho_{e,x}a_{sc}$ can be achieved [3]. With the use of scaled Hounsfield units and water as reference material the equation can be equaled to unity. By definition $H_1 = H_2 = 1000$, this can be plugged in and we can end up with equation 13 for the relative electron density of the tissue compared to water. See [3] for a detailed description of the derivation.

$$\frac{\rho_{e,x}}{\rho_{e,H_2O}} = a\Big(\frac{H_1}{1000}\Big) + (1-a)\Big(\frac{H_2}{1000}\Big) \tag{13}$$

where,

$$a = \Big(\frac{1}{\rho_{e,H_2O}a_{sc}}\Big)\frac{\overline{f}_2\overline{\mu}_{H_2O,1}}{\overline{g}_1\overline{f}_2 - \overline{g}_2\overline{f}_1} \tag{14}$$

In a similar manner the equation for the effective atomic number Z_x for a calibration material x can be extracted. This is done by introducing a second constant b. We again refer to [3] for a detailed description of the derivation.

$$\frac{\rho_{e,x}}{\rho_{e,H_2O}}Z_x^n = b\Big(\frac{H_1}{1000}\Big) + (Z_{H_2O}^n - b)\Big(\frac{H_2}{1000}\Big) \tag{15}$$

where,

$$b = \Big(\frac{1}{a_{pe}\rho_{e,H_2O}}\Big)\frac{\overline{g}_2\overline{\mu}_{H_2O,1}}{\overline{g}_2\overline{f}_1 - \overline{g}_1\overline{f}_2} \tag{16}$$

To obtain the electron density for a mixture of atoms with a certain effective atomic number equation 17 can be used. In this equation ρ_e is the electron density in the composed material. $\rho_{e,i}$ denotes the contribution of the atom type i to the total electron density [11].

$$\rho_e Z_x^n = \sum_i \rho_{e,i} Z_i^n \tag{17}$$

An expression for the effective atomic number expressed in terms of the composed atomic numbers and the mass fractions can be found. See [3] for a complete derivation.

$$Z_x = \left(\frac{\sum_i \frac{w_i Z_i}{A_i} Z_i^n}{\sum_i \frac{w_i Z_i}{A_i}} \right)^{1/n} \tag{18}$$

This definition can be used to calculate the effective atomic number in equation 15. However the coefficient n should be determined beforehand. Hünemohr [11] determined the coefficient n by x-ray absorption simulations, which indicate that the optimum coefficient lies around n=3.1. This is done for a Z range of 1 to 20.

3 Method

In this report the accuracy of the determination of proton stopping powers is investigated. The determination is done with the use of a dual energy CT. Two distinct pairs of low (30-60 keV) and high (90-150 keV) tube voltages will be used to determine the effective atomic number (Z_{eff}) and the relative electron density (RED). The difference in accuracy of both tube voltage pairs will be compared. The Z_{eff} and RED will be calculated with the constants a and b given in formulas 13 and 15. The constants are determined first, with a calibration material which is chosen to be the best by [3] to be AlMgSil.
For this experiment two data sets of materials will be used, from which the composition and the density information are known. The first data set contains 39 materials, which are introduced by [12]. The second data set consists of 81 human tissues [13]. From NIST the atomic cross section is taken as a function of photon energy [14]. With the use of SpekCalc the x-ray spectra will be calculated for all tube voltages from 30 to 150 kV with steps of 10 kV. The filtration parameters in SpekCalc will be set on 3 mm aluminum, 500 mm air and 0.9 mm titanium and the anode angle on 8°.

3.1 The Hounsfield units

In practice a dual energy CT will provide the Hounsfield units for every sample. However, in this investigation a practical CT scan will not be used, but the Hounsfield units for all the materials will be calculated with equation 8 and the composition of the materials. In order to obtain the scaled Hounsfield units the attenuation coefficients for all separate materials are needed. The attenuation coefficient for a specific material x is given by: $\mu_x = \rho_e \sigma_e(E)$. In which ρ_e is the electron density and $\sigma_e(E)$ is the electronic cross-section, which is dependent on the photon energy. The electron density determined by the composition of the material. The electron density $\rho_{e,i}$ for a specific element i are given by the following equation [3]:

$$\rho_{e,i} = \frac{\rho_x N_A}{M_u} \omega_i \frac{Z_i}{A_i} \tag{19}$$

N_A is the Avogadro's constant and M_u is the molar mass constant. Z_i and A_i give the atomic number and atomic mass for a specific element i, respectively. The mass fraction of a specific

element i relative to the total mass of the material, is given by ω_i. To get the average attenuation for a material, $\rho_{e,i}$ needs to be summed over all the elements i and photon energies k:

$$\overline{\mu}_{x,j} = \frac{\rho_x N_A}{M_u} \sum_{k=1}^{N} w_{j,k} \left(\sum_i \frac{\omega_i Z_i}{A_i} \left(\frac{\sigma_{i,k}}{Z_i} \right) \right) \tag{20}$$

w_j is the energy distribution of the x-ray spectrum given in equation 10. In this report the energy dependence of the detector will not be taken in to account, due to the small influence.
With the use of the composition of the materials and the spectrum all average attenuation coefficients can be calculated. From these coefficients the Hounsfield units will be extracted with equation 8.

3.2 The relative electron density

According to equation 13 the relative electron density can be calculated with the use of the two Hounsfield units of the dual energy CT and the constant a. However the constant a is still undetermined. The constant can be calculated with the use of a calibration material. The calibration material is chosen to be AlMgSi1, because then the difference in the calculated RED and the real RED from the composition of the material was found to be the smallest in an earlier study [3]. This constant will be calculated separately for both pairs of tube voltages. With this constant the RED's will be calculated for all the different materials. These will be compared to the real relative electron densities known from the composition of the materials. The accuracy of both obtained sets of RED's for the different tube voltage pairs will be compared.

3.3 The effective atomic number

With the use of equation 1 and the Hounsfield unit pairs the effective atomic number Z_x can be calculated. Constant b can be determined with the same method as constant a, again with the calibration material AlMgSi1 [3]. However, equation 1 also depends on the parameter n, which according to [3] lies close to 3.3. Because the parameter n can be energy dependent, b will be calculated for the voltage pairs separately, with n ranging from $n = 2.6$ until $n = 3.5$ with steps of 0.05. With b the effective atomic number can be calculated. This effective atomic number will be compared to the atomic number from 18, so that the best value of n can be chosen for the corresponding voltage pairs.

The values which are found for a, b and n will be used for both, the data set of the various materials and the data set of the human tissues.

3.4 Noise on the Hounsfield units

During a real CT-scan, noise will be present in the Hounsfield units, due to statistical fluctuations. The Hounsfield units determined with the method described in section 3.1 do not include noise, due to the calculation approach. To investigate the accuracy, noise should be taken into account. This will be done by introducing noise to the Hounsfield units of six different tissues. The tissues which are chosen are: inflated lung, adiopose 2, liver 2, muscle 2, cortical bone and total bone. To introduce noise, a value will be added and subtracted to all Hounsfield units. According to Hünemohr [11], who obtained the data from real CT-scans the noise value should be chosen to be around 10 HU. With the new Hounsfield units the relative electron density and the effective atomic number will be calculated. This will be done for pairs where for both 10 HU is added or subtracted. It will also be

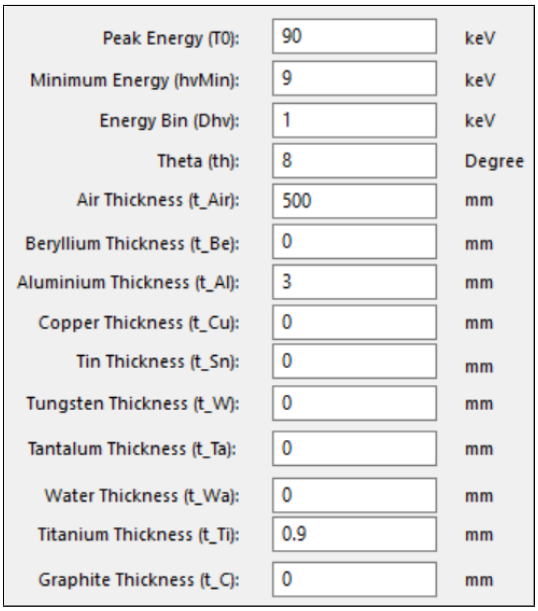

Peak Energy (T0):	90	keV
Minimum Energy (hvMin):	9	keV
Energy Bin (Dhv):	1	keV
Theta (th):	8	Degree
Air Thickness (t_Air):	500	mm
Beryllium Thickness (t_Be):	0	mm
Aluminium Thickness (t_Al):	3	mm
Copper Thickness (t_Cu):	0	mm
Tin Thickness (t_Sn):	0	mm
Tungsten Thickness (t_W):	0	mm
Tantalum Thickness (t_Ta):	0	mm
Water Thickness (t_Wa):	0	mm
Titanium Thickness (t_Ti):	0.9	mm
Graphite Thickness (t_C):	0	mm

Figure 4 – The SpekCalc setting panel for a tube voltage of 90 kV

done for pairs, where for one 10 HU is added and for the other 10 HU is subtracted and vice versa. Now the accuracy of the RED's and the Z_{eff} of both tube voltage pairs can be compared.

4 Results

SpekCalc is used to calculate the x-ray spectra for the tube voltages ranging from 30 kV until 150 kV, with steps of 10 kV. To get the best convention with a siemens CT-scan [9], the filters were set on 3 mm aluminum, 500 mm air and 0.9 mm titanium and the anode angle was set on 8°. An overview of the settings for a tube voltage of 90 kV is given in figure 4. In figure 5 two examples of the x-ray spectra are shown, for tube voltages of for 90 kV (green) and 150 kV (red).

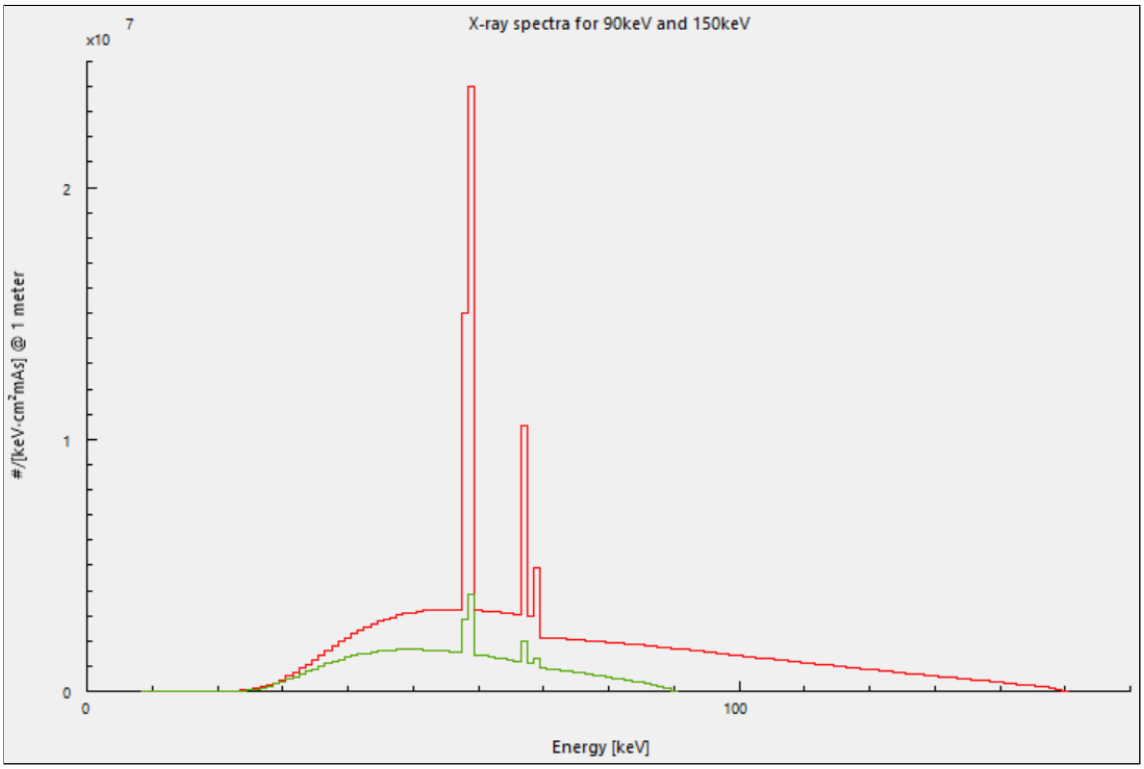

Figure 5 – The x-ray spectra for both tube voltages 90 kV and 150 kV coloured in green and red, respectively. The horizontal axis shows the photon energy in units of keV. The vertical axis shows the number of photons counted for the specific energy in units of keV· cm^2· mAs.

4.1 The Hounsfield units

With the use of the composition of the materials and tissues, given by [12] [13], the fractional electron density could be calculated. This is the electron density that can be attributed to a specific element in a material (equation 19). To calculate the average attenuation of the photons in the materials and tissues, for a tube voltage j, equation 20 is used. Here, the spectrum for the tube voltage is obtained from SpekCalc and this spectrum was then normalized. The average attenuation is used to determine all the scaled Hounsfield units for differing tube voltages. The Hounsfield units are all calculated with equation 8 and are stated in tables 18 and 19 of the appendix.

4.2 The relative electron densities of the materials

The Hounsfield units found for AlMgSi1 and equation 13 are used to extract a. a is dependent on the reference material and the tube voltage. All a values used during the calculations are given in table 1. From here the RED's are calculated, for convention these will be called RED_{calc}. Due to different a values and Hounsfield units the RED_{calc} differ per tube voltage pair. In figure 6 the ratio of RED_{calc} over RED_{real} is plotted, for two different tube voltage pairs.

Tube voltage (kV)	Reference material	a	n	b
30/60	AlMgSi1	1.94	3.25	-954
30/60	CB2-30%	1.98	3.20	-855
60/100	CB2-30%	2.55	3.25	-4587
90/150	AlMgSi1	3.07	3.30	-10532

Table 1 – Values for a, n and b, which are used to calculate the relative electron densities and the effective atomic numbers of the tissues.

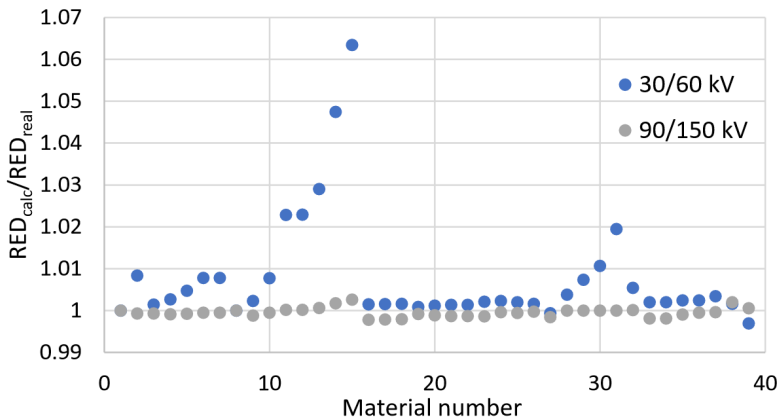

Figure 6 – Plot of the accuracy of determining the relative electron densities with tube voltage pairs of 30/60 kV and 90/150 kV. On the vertical axis the ratio is given between the calculated RED and the real RED. The horizontal axis shows the material number.

In the ideal case $\mathrm{RED_{calc}/RED_{real}}$=1. From figure 6 it can be seen that $\mathrm{RED_{calc}/RED_{real}}$ has a maximum deviation of less than 1% for a tube voltage pair of 90/150 kV. However, for a tube voltage pair of 30/60 kV there is almost a maximum deviation of 7%. This deviation occurs especially at material numbers 13, 14, and 15, which correspond to the materials CB2-30%, CB2-50% and SB3.

To obviate this deviation CB2-30% was taken as reference material as well. The a value which is obtained is given in table 1. A new graph is made to compare the accuracy of the relative electron densities for the tube voltage pair 30/60 kV, obtained with reference materials AlMgSi1 and CB2-30%. The data is plot in figure 7.

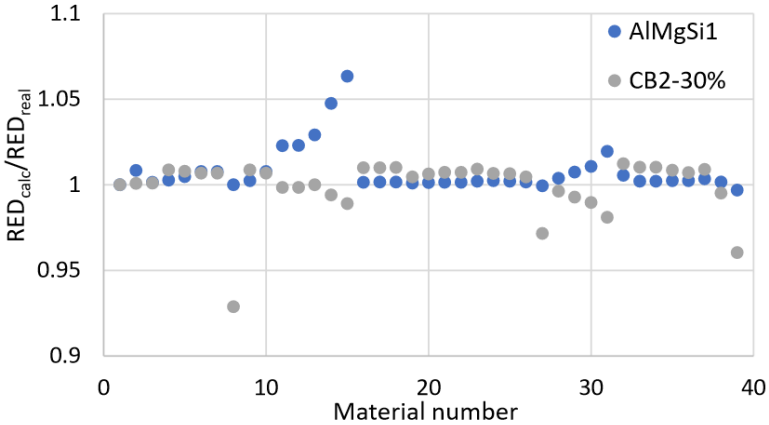

Figure 7 – Plot of the accuracy of determining the relative electron densities for a tube voltage pair of 30/60 kV. Both reference materials AlMgSi1 and CB2-30% are used. On the vertical axis the ratio between $\mathrm{RED}_{\mathrm{calc}}$ and $\mathrm{RED}_{\mathrm{real}}$ is given. The horizontal axis shows the material number.

From figure 7 it is remarkable that the deviations are all above 1 for the reference material AlMgSi1. However, the large deviations with CB2-30% as reference material are smaller than 1.

To increase the accuracy the analysis is done with an a higher tube voltage. The highest tube voltage is chosen to be 100 kV. The best value for the low tube voltage is chosen with the method described below:
In a real CT-scanner noise will be present in the Hounsfield units. According to equation 13, the difference between H_1 and H_2 is important for the calculation of the relative electron densities. However, when noise is present this difference will be affected even more, especially when the difference between the Hounsfield units is already small. To make sure the Hounsfield units differ enough, the tube voltages need to be chosen apart from each other. To calculate the influence of noise on the Hounsfield units, error analysis is done. The error in the relative electron density, $\Delta\rho$, due to fluctuations in the Hounsfield units can be calculated with equation 21. In a previous study [11] is concluded that the average noise value in the Hounsfield units lie around 10. This error is used, together with the value of a (table 1) to calculate the $\Delta\rho$ for the tube voltage pair 90/150 kV. Now, the new low tube voltage is chosen in such a way that the associated $\Delta\rho$ is smaller than the $\Delta\rho$ for the voltage pair 90/150 kV. It is concluded that for a voltage pair of 60/100 kV, the Hounsfield units will be far enough apart to prevent the noise to interfere.

$$\Delta\rho = \left(\frac{a}{1000}\right)^2 \Delta H_1^2 + \left(\frac{1-a}{1000}\right)^2 \Delta H_2^2 \tag{21}$$

To test the accuracy of the voltage pair 60/100 kV, $\mathrm{RED}_{\mathrm{calc}}/\mathrm{RED}_{\mathrm{real}}$ is plotted for all the materials (figure 8). The relative electron densities are calculated with both reference materials AlMgSi1 and CB2-30%. If this graph is compared to figure 7, it can be observed that the accuracy increased with the higher voltage pair.

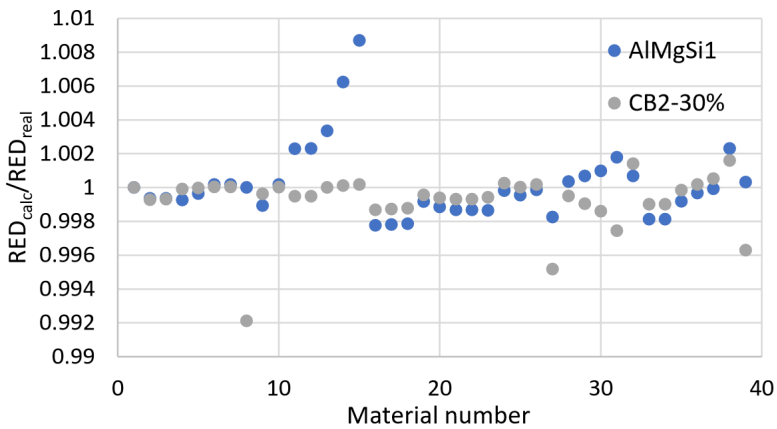

Figure 8 – Plot of the accuracy of determining the relative electron densities for a tube voltage pair of 60/100 kV. Both reference materials AlMgSi1 and CB2-30% are used. On the vertical axis the ratio between $\mathrm{RED_{calc}}$ and $\mathrm{RED_{real}}$ is given. The horizontal axis shows the material number.

To be sure which reference material gives the smallest error in the relative electron density, the average fluctuation of $\mathrm{RED_{calc}}/\mathrm{RED_{real}}$ around 1 is calculated. It is observed that the relative electron densities calculated with the reference material CB2-30% has the smallest fluctuations around 1.

4.3 The relative electron density of the tissues

Since a has already been determined with the materials in section 4.2, the relative electron densities of the tissues can directly be calculated. This is done for the tube voltage settings: 30/60 kV, 60/100 kV and 90/150 kV and reference materials: AlMgSi1 and CB2-30%. The values used for a can be found in table 1.

The relative electron densities for the tissues were calculated with equation 13. The relative electron densities over the real relative electron densities were plotted versus the material number (figure 9). It is observed that after tissue 53 the relative electron density is less accurate. It should be noticed, from table 17 in the appendix, that the tissues with a material number larger than 53 are more dense tissues, like bone. In figure 9a $\mathrm{RED_{calc}}/\mathrm{RED_{real}}$ is plotted, determined with a tube voltage of 30/60 kV. The blue and grey data points are calculated with reference materials AlMgSi1 and CB2-30%, respectively. Again the $\mathrm{RED_{calc}}/\mathrm{RED_{real}}$ calculated with CB2-30% lies below 1 and the $\mathrm{RED_{calc}}/\mathrm{RED_{real}}$ calculated with AlMgSi1 lies above 1. It should be noticed that the distribution of the vertical axis in figure 9b is changed and that the data points are closer to 1.

To investigate the dependence of the relative electron density on the difference in the Hounsfield units a graph is made (figure**??**). In this graph $\mathrm{RED_{calc}}/\mathrm{RED_{real}}$ is plot versus $\Delta H = H_1 - H_2$. This is done for both the data sets obtained with 30/60 kV and reference materials AlMgSi1 and CB2-30%. It can be observed that there is a noticeable correlation between $\mathrm{RED_{calc}}/\mathrm{RED_{real}}$ and ΔH. To use this correlation a linear fit is made through the data points with $\Delta H <$ -500. This is shown in figure 10. The equations for both fits are given in the figure. The largest deviating tissue, which is skeleton-cortical bone, has a Hounsfield unit difference of -3047. The equation corresponding to reference material CB2-30% is used to scale the relative electron density. The relative electron density is scaled by a factor of 0.9756. With this method we obtain an accuracy of 0.3% for the largest deviating tissue skeleton-cortical bone.

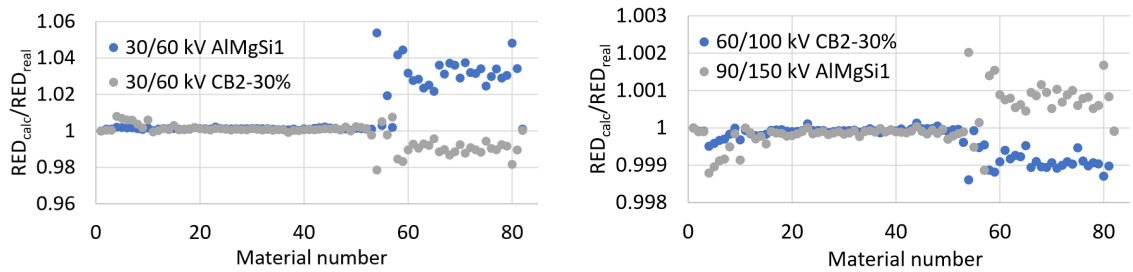

(a) (b)

Figure 9 – Plot of the accuracy of determining the relative electron densities for the tube voltage pairs of 30/60 kV, 60/100 kV and 90/150 kV. Both reference materials AlMgSi1 and CB2-30% are used. On the vertical axis the ratio between $\mathrm{RED_{calc}}$ and $\mathrm{RED_{real}}$ is given. The horizontal axis shows the type of tissue.

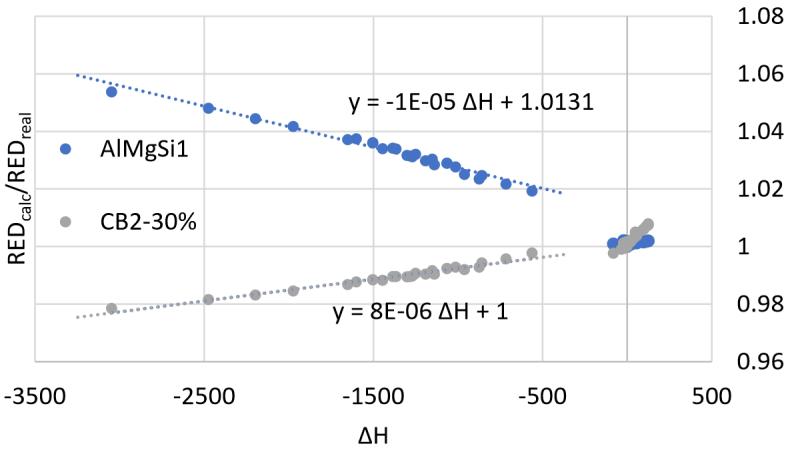

Figure 10 – Plot of the accuracy of relative electron densities for the tube voltage pair 30/60 kV. Both reference materials AlMgSi1 and CB2-30% are used. On the vertical axis the ratio between $\mathrm{RED_{calc}}$ and $\mathrm{RED_{real}}$ is given. The horizontal axis shows difference in Hounsfield units. A line is fit through the correlation between the RED and the ΔH for $\Delta H < -500$

4.4 The effective atomic numbers of the materials

For the effective atomic number, Z_x, three different voltage pairs and both reference materials, found in section 4.2, are used. All the different settings can be found in table 1. Before Z_x could be obtained, b needed to be determined. This was done with equation 15, with n still as a variable ranging from 2.6 till 3.5. Z_x and Z_{H_2O} were both found with equation 18. The values found for b are given in table 1. From here Z_x could be determined as a function of n. To find the best value for n, the calculated Z_x is compared with the Z obtained with equation 18. From now on this later Z is called the true atomic number, Z_{true}. The comparison between the two Z values is done by calculating the root mean square deviation (RMSD), given in equation 22.

$$\mathrm{RMSD} = \frac{1}{N}\sqrt{\sum_x \left(\frac{Z_x - Z_{x,\mathrm{true}}}{Z_{x,\mathrm{true}}}\right)^2} \tag{22}$$

In this equation is summed over all the materials, x. N is used for the total amount of materials. The n value is chosen for which the RMSD is the lowest. In figure 21 of the appendix the RMSD is plot versus the n value. The most favourable n value is found to be n=3.20 for the tube voltage 30/60 kV with CB2-30% as reference material. For the tube voltages 30/60 and 60/100 kV, with reference materials AlMgSi1 and CB2-30%, respectively, n is found to be 3.25. For the last tube voltage pair, 90/150 kV, the RMSD is found to be the smallest for n=3.30.

To investigate the accuracy of the effective atomic numbers graphs are made, which are shown in figure 11. In these graphs the left vertical axis shows the obtained Z_x and the right vertical axis shows the difference, Z_{true}-Z_x. These are both plot versus Z_{true}. This is done for all four of the settings. From the blue graph, which shows Z_x, it can be observed that the data points have a higher fluctuation in 11a and 11b compared to 11d. Looking at the grey data points, this effect becomes better observable. In 11a the data points are more spread out and in 11c and 11d the points are more focused around the line ΔZ=0. It should be noticed that the range on the axis for ΔZ is changed in 11b. This is done because the data points go to lower values.

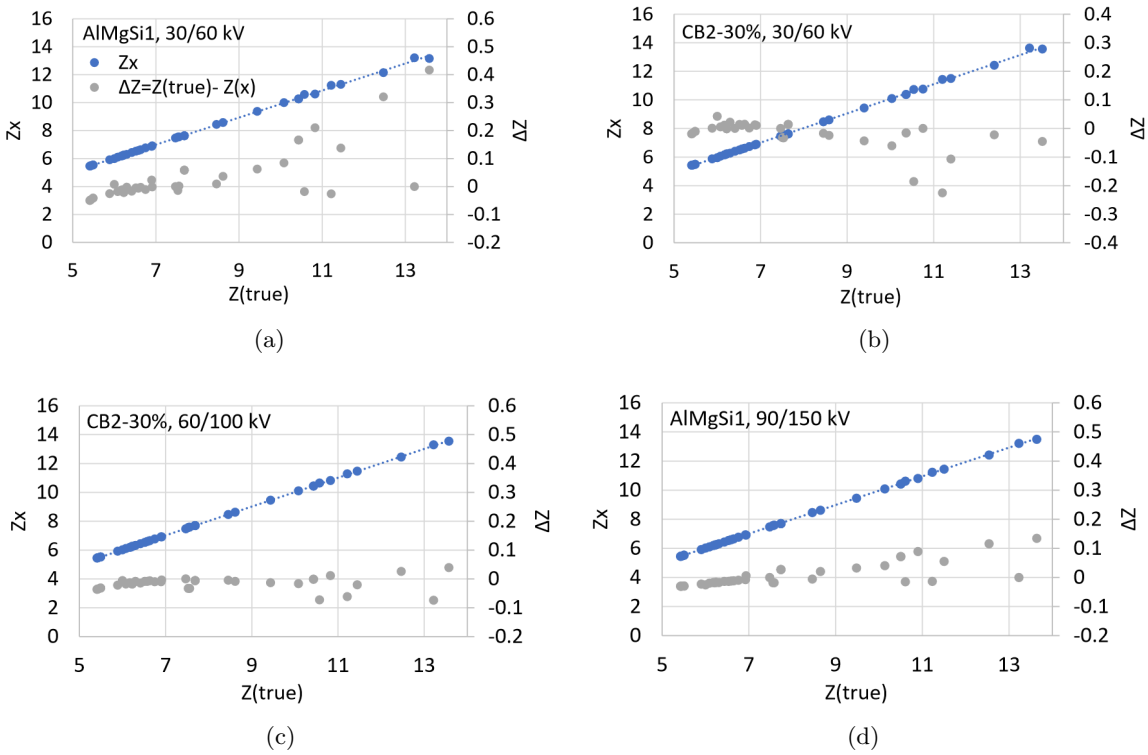

Figure 11 – Correctness of Z_x. The left vertical axis shows the obtained Z_x and the right vertical axis shows the difference, Z_{true}-Z_x. The horizontal axis shows Z_{true}.

4.5 The effective atomic numbers of the tissues

The effective atomic numbers of all the tissues are calculated with table 1 and equation 15. Here Z_{H_2O} is obtained with the composition of water and equation 18. To illustrate the accuracy of Z_x graphs are made in figure 12. On the vertical axis the difference between Z_x and Z_{true} (obtained with equation 18) is shown. On the horizontal axis the tissue number is shown, which can be found in table 17 of the appendix. It should be noticed that the range on the vertical axis is changed. For the reference material AlMgSi1 the maximum deviation is found to be 0.35 and for the reference material CB2-30% it is found to be 0.11, both for a tube voltage pair of 30/60 kV.

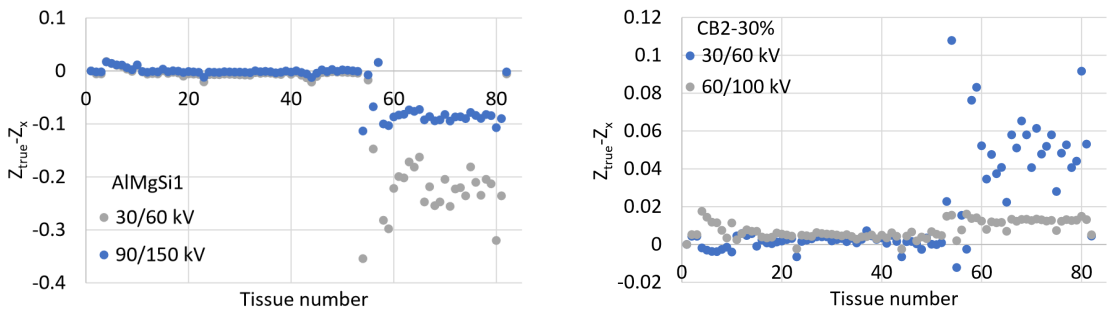

(a) (b)

Figure 12 – The correctness of the effective atomic number. The vertical axis shows the deviation from the real effective atomic number. The horizontal axis shows the number of the tissue.

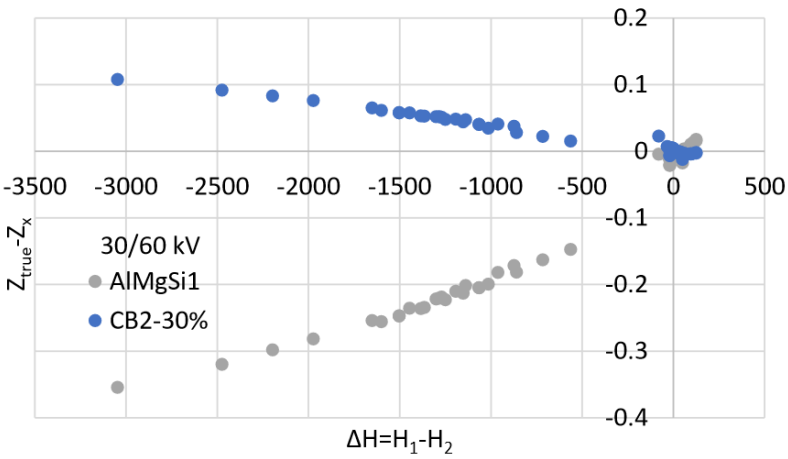

Figure 13 – The correctness of the effective atomic number compared to the Hounsfield unit difference. The vertical axis shows the deviation from the real effective atomic number. The horizontal axis shows $\Delta H = H_1 - H_2$

Again a correlation was found between the difference in Hounsfield units and the correctness of the effective atomic number. For both reference materials the correlation is plotted, both with a tube voltage pair of 30/60 kV (figure 13). The grey and the blue data points from figures 12a and 12b, respectively, are plotted in this figure. The effective atomic number depends on the relative electron density, equation 15. It was found that the deviation of the relative electron density influences the effective atomic number. If the relative electron density was scaled with the correlation curve 10, the effective atomic number becomes more accurate. This was found to be true for the most deviating tissue skeleton cortical bone. The method which is used is explained below:

From figure 13 it can be seen that the most deviating tissue (for both reference materials) has a Hounsfield unit difference of -3047. This corresponds to the material skeleton-cortical bone. From figure 10 the correlation curves could be observed. If the relative electron density of skeleton cortical bone was scaled by this curve it influenced the accuracy the effective atomic number. It was found that effective atomic number was in between 0.01 accuracy of the Z_x for skeleton cortical bone with the reference material CB2-30%.

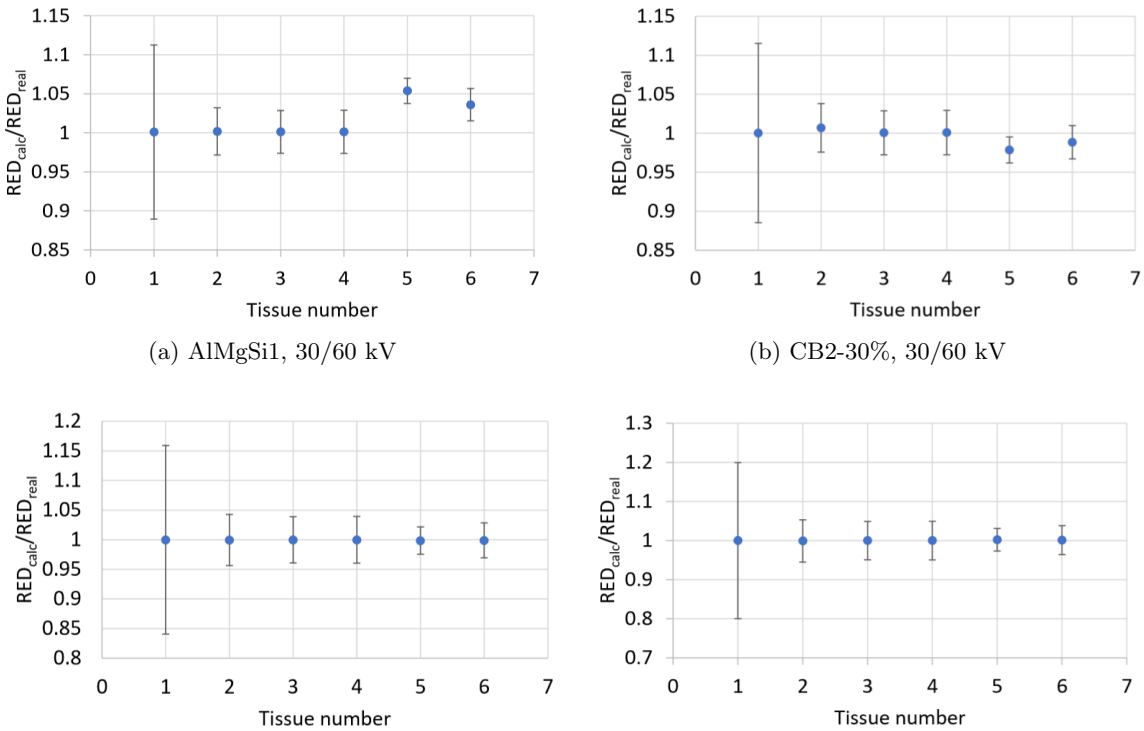

(a) AlMgSi1, 30/60 kV

(b) CB2-30%, 30/60 kV

(c) CB2-30%, 60/100 kV

(d) AlMgSi1, 90/150 kV

Figure 14 – The accuracy of the relative electron density when noise is introduced. The blue data points show the calculated RED and the error bars show the possible deviations when noise is present.

4.6 Noise on the Hounsfield units

To study the effect of noise on the Hounsfield units, noise is added to the Hounsfield units. This is done by adding and subtracting of a value of 10 on the Hounsfield units. This study was done for six different tissues. The tissues which were chosen are: lung-inflated, adiopose tissue 2, liver 2, muscle skeletal 2, skeleton-cortical bone, humerus (total bone). The new obtained Hounsfield units are given in table 20 of the appendix.

It was found that for all tissues the calculated relative electron density becomes larger when 10 HU is added to H_1 and 10 is subtracted from H_2. In contrary the relative electron density becomes smaller when 10 HU is subtracted from H_1 and 10 HU is added to H_2. Figure 14 visualizes the deviation of the relative electron density with noise present. In these figures the vertical axis shows the ratio between RED_{calc} and RED_{real}. The horizontal axis shows the type of tissue, which can be found in table 20. The blue dots indicate the ratio which is found with the Hounsfield units without noise. Since the calculated value of the RED can be different than the real RED not all blue dots lie on the line $\text{RED}_{\text{calc}}/\text{RED}_{\text{real}}=1$. The error bars indicate the range of the deviation, when a noise value of 10 HU is present. It should be noticed that the range on the vertical axis is changed for figure 14c and figure 14d. It is observable that the calculated RED becomes more accurate when the tube voltage is increased. However, at the same time the magnitude of the deviations (the error bars) increase.

The effect of noise on the effective atomic number is shown in figure 15. In the plots the blue data points illustrate the calculated effective atomic number. The error bars show the range of fluctuations around the Z_x for a noise value of 10. It should be noticed that the range on the vertical axis in figure 15c and figure 15d has changed. It was found that when 10 HU was added to

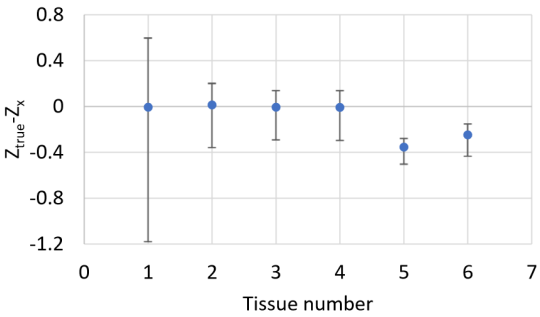

(a) AlMgSi1, 30/60 kV

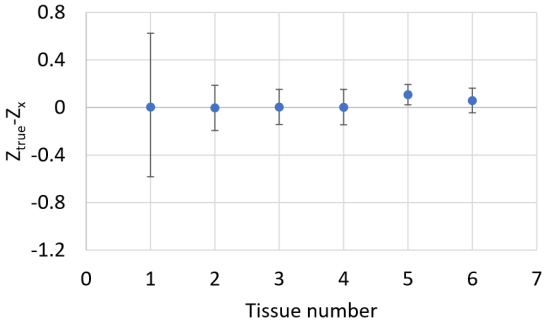

(b) CB2-30%, 30/60 kV

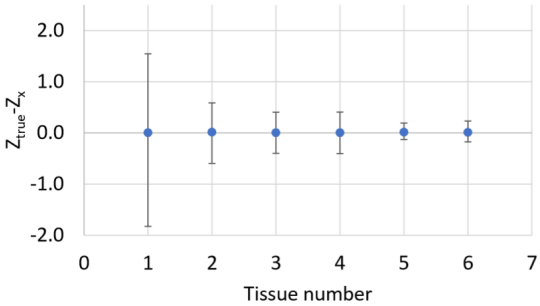

(c) CB2-30%, 60/100kV

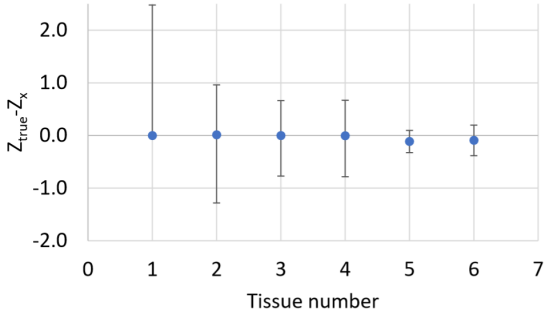

(d) AlMgSi1, 90/150 kV

Figure 15 – The correctness of the effective atomic number when noise is introduced. The blue data points show the calculated effective atomic number and the error bars show the possible deviations when noise is present.

H_1 and 10 HU was subtracted from H_2 that the calculated effective atomic number became smaller. The opposite effect happened when 10 HU was subtracted from H_1 and 10 HU was added to H_2. From the graphs it can be seen that deviation of Z_x around Z_{true} decreases when the tube voltage is increased. However, the magnitude of the fluctuations around Z_x increased.

5 Discussion

In the first part the relative electron densities of the materials are determined with the reference material AlMgSi1. This was done for both tube voltage pairs 30/60 kV and 90/150 kV, figure 6. It was found that the accuracy deteriorated significantly with a lower tube voltage. For bone-like structures there was a deviation of 7%, which is too large to use for the determination of the proton stopping power.
CB2-30% was used as reference material as well. From figure 7 it can be observed that the relative electron densities estimated with AlMgSi1 are too large and with CB2-30% are too small. This effect has to do with strength of the attenuation coefficient compared to water and it is further explained in appendix 7.3. The overall accuracy of the RED of the materials did not change. However, the materials for which the deviation occurred did. The largest deviations occurred with the materials: AlMgSi1, Silicon oil Siluron 5000, Potassiom chloride sol and Al2O3 99.7%. Since these materials are not present in the human body, CB2-30% is chosen as the best reference material to use for the calculation of the relative electron density.
To further investigate the effect of the tube voltage, it is increased to 60/100 kV. For the reference material AlMgSi1 an accuracy of 1% is found and for the reference material CB2-30% an accuracy of 0.2% (if the four materials mentioned before were not taken into account). In comparison to the high tube voltage of 90/150 kV, it is almost the same accuracy. The tube voltage 90/150 kV has an accuracy of 0.2% (figure 6).
In the next part the relative electron densities of the tissues are determined. Again this was done for the tube voltage pair of 30/60 kV and both reference materials AlMgSi1 and CB2-30%. Once more the electron densities obtained with the reference material AlMgSi1 turned out less accurate than the electron densities obtained with CB2-30%. With the reference material CB2-30% an accuracy of 2% was obtained.
For both sets of relative electron densities we found a linear correlation with the difference in the Hounsfield units. Since the reference material CB2-30% shows a higher accuracy this material is preferred for further calculations. With the use of the equation in figure 10 it is possible to obtain an accuracy of 0.3% for the largest deviating tissue skeleton-cortical bone, with a tube voltage of 30/60 kV. To calculate the factor, which is used to scale the RED, the difference in Hounsfield units is used. This means that noise has an amplified effect on this factor. So the influence of noise needs to be studied. According to [11] the value of noise lies around 10. This means that ΔH can differ with 20. With the use of the equations in figure 10 it is found that this will have an influence of 0.03% on the accuracy if the relative electron density. It is concluded that noise will not have a significant effect on this method. This research is done with 82 human tissues, however, other tissues may exist which are not consistent with the fit. Before the method is used the tissues present in the irradiated part need to be compared with these 82 tissues.
Equation 15 is used to determine the effective atomic numbers of the materials and the tissues. In this equation there were two variables present: n and b. In previous studies n was approximated to be 3.3. Here the n values found were: 3.20, 3.25 and 3.30, in agreement with earlier studies. The correctness of the effective atomic number can be found in figure 11 and 12, for the materials and tissues, respectively. It is observed that the correctness decreased with an decreasing tube voltage. In figure 13 the correctness of both reference materials, with a tube voltage pair of 30/60 kV, is compared. The atomic numbers achieved with the reference material CB2-30% turned out to be closer to the atomic number calculated with equation 18. A maximum difference of 0.1 is found for the tissue skeleton - cortical bone. From the same figure 13 a correlation is observed with the difference in Hounsfield. This is due to the fact that the effective atomic number depends on the relative electron density. When the relative electron density was scaled for the ratio found in figure 10 the correctness of the Z_x of skeleton - cortical bone increased to 0.01.
For the relative electron density and the effective atomic number the influence of noise on the Hounsfield units is tested. From the previous discussion the tube voltage pair of 30/60 kV and the reference material CB2-30% was considered as a reliable set-up. To test the influence of noise these settings were compared to the voltage pair of 90/150 kV with reference material AlMgSi1. For the

relative electron density the figures 14b and 14d are compared and for the effective atomic number the figures 15b and 15d. It is found that the accuracy increased with a lower tube voltage. This can be explained by the behaviour of the linear attenuation coefficient with a lower tube voltage (Chapter 8 in [5]). This behaviour induces that the ΔH for a lower tube voltage pair is larger than the ΔH for a higher tube voltage pair. This means that the influence of noise on the ΔH decreases with a lower tube voltage pair and so the accuracy will increase. However, this method was based on a noise value obtained from a 100/140 kV dual energy CT. When a lower tube voltage is used the noise value may differ. This means that the influence of noise on the obtained electron density and effective atomic number can be different. Before a low kV dual energy CT is used in preclinical research, research needs to be done into the noise on low kV CT scans.
From figures 14 and 15 it is also observed that the error range for the first tissue is much higher than for the other tissues. This tissue corresponds to an inflated lung. Errors of 10% and 0.6 were found for the relative electron density and the effective atomic number, respectively. These errors would normally be too large to use for the calculation of the proton stopping power. However, the density of an inflated lung is very low and so the proton energy transfer will be too. A relative large error in a low proton energy transfer will not effect the absolute proton energy significantly. This means that the absolute proton energy can still be approximated accurate enough, to use for the proton stopping power.
When the energy of a photon decreases, the interaction probability with the tissue will increase [5]. This means that the signal which reaches the detector will be lower and so the efficiency will drop if the tube voltage is decreased. To overcome this effect, the current going through the cathode in the x-ray tube needs to be increased. This will enhance the amount of photons reaching the detector. However, at the same time the dose will increase, which is unwanted. So before dual energy CT will be tested in preclinical research, more research needs to be done into the efficiency of using a tube voltage pair of 30/60 kV.

6 Conclusion

In this research the accuracy of the use of a low kV dual energy CT for the determination of proton stopping power was investigated. It is explained how the proton stopping power can be calculated, from the electron density and the effective atomic number of the tissue, obtained with a dual energy CT-scan. In this report the accuracy of the electron density and the effective atomic number obtained with a 30/60 kV dual energy CT was investigated.
Firstly, it was concluded that a voltage pair of 30/60 kV, with reference material AlMgSi1, was not accurate enough to use for the determination of the proton stopping power. The deviation of the relative electron density and the correctness of the effective atomic number were 7% and 0.35, respectively. It was found that the reference material CB2-30% gave more accurate results. The deviation of the relative electron density and the correctness of the effective atomic number were 2% and 0.12, respectively.
A correlation was observed between the difference in Hounsfield units (using equation 13) and the accuracy of the relative electron density. The accuracy was increased if it was scaled by the correlation curve. This resulted in a positive effect on the correctness of the effective atomic number. The new deviation of the relative electron density and the correctness of the effective atomic number were 0.3% and 0.02. This can be compared to the accuracy of a 90/150 kV dual energy CT, which shows the values 0.2% and 0.1. It is concluded that the tube voltage of 30/60kV shows a reasonable accuracy to use for the determination of the proton stopping power.
The influence of noise on the Hounsfield units was investigated as well. It was observed that the influence decreases, if a lower tube voltage pair is chosen. However, the noise value was based on a 100/140 kV dual energy CT scan. In further research this value should be based on a low kV dual energy CT scan. Moreover, this research did not go into depth about the efficiency of a low kV dual energy CT. The signal reaching the detector will drop if the voltage is decreased. To detect

enough photons the dose needs to be increased possibly to an unfavourable high level. Before a low kilo-voltage dual energy CT is used in preclinical research a consideration needs to be made between the essential signal and the dose.
From the overall research it can be concluded that a low tube voltage of 30/60 kV can be used, with reference material CB2-30%. However, before the determination of the proton stopping powers with a dual energy CT can be tested, research needs to be done into the efficiency and the noise of low kV dual energy CT-scans.

References

[1] H. Paganetti, *Proton Therapy Physics.* CRC Press, second ed., 2019.

[2] Wikipedia, "Hounsfield scale," 2010. `https://en.wikipedia.org/wiki/Hounsfield_scale`, accessed on: 04-06-2019.

[3] E. R. van der Graaf, "Converting SECT and DECT information into proton stopping powers," June 2016. KVI-CART internal report.

[4] J. M. Boone, O. Velazquez, and S. R. Cherry, "Small-animal x-ray dose from micro-ct," *Molecular Physics*, vol. 3, no. 3, pp. 149–158, 2004.

[5] J. E. Turner, *Atoms, Radiation, and Radiation Protection.* WILEY-VCH Verlag GmbH & Co. KGaA, third ed., 2007.

[6] H. O. Tekin and U. Kara, "Analysis of filtering material and its effect on X-ray features by using monte carlo method for medical imaging applications," *The Open Orthopaedics Journal*, pp. 1500–1520, 2017.

[7] PhysicsOpenLab, "Bremsstrahlung radiation," 2017. `http://physicsopenlab.org/2017/08/02/bremsstrahlung-radiation/`, accessed on: 09-06-2019.

[8] G. Poludniowski *et al.*, "SpekCalc: A program to calculate photon spectra from tungsten anode x-ray tubes," *Physics in Medicine & Biology*, vol. 54, pp. N433–N438, 2009.

[9] H. A. Duisterwinkel *et al.*, "Spectra of clinical CT scanners using a portable compton spectrometer," *Medical Physics*, vol. 42, no. 4, pp. 1884–1894, 2015.

[10] P. Mah, T. E. Reeves, and W. D. McDavid, "Deriving Hounsfield units using grey levels in cone beam computed tomography," *The British Institute of Radiology*, pp. 323–335, 2010.

[11] N. Hünemohr *et al.*, "Experimental verification of ion stopping power prediction from dual energy ct data in tissue surrogates," *Physics in Medicine & Biology*, 2014.

[12] J. van Abbema *et al.*, *Accurate relative stopping power prediction from dual energy CT for proton therapy.* University of Groningen, first ed., 2017.

[13] D. R. White, H. Q. Woodard, and S. M. Hammond, "Average soft-tissue and bone models for use in radiation dosimetry," *The British journal of radiology*, vol. 60, no. 717, pp. 907–913, 1987.

[14] NIST, "Xcom: Photon cross sections database," 2010. `https://www.nist.gov/pml/xcom-photon-cross-sections-database`, accesed on: 03-2019.

[15] G. Matscheko, G. A. Carlsson, and R. Ribberfors, "Compton spectroscopy in the diagnostic x-ray energy range: II. effects of scattering material and energy resolution," *Physics in Medicine & Biology*, vol. 34, no. 2, p. 199, 1989.

7 Appendix

7.1 Type of materials and tissues

1	water	14	CB2-50%	27	Silicon oil Siluron 5000
2	LN300	15	SB3	28	Potassium Chloride sol 1:5
3	LN450	16	n-Pentane	29	Potassium Chloride sol 1:2
4	AP6	17	n-Hexan	30	Potassium Chloride sol 1:1
5	BR12	18	n-Heptane	31	Potassium Chloride sol
6	CT SW	19	Methanol	32	Carbon
7	SW M457	20	Ethanol	33	UHMWPE
8	AlMgSi1	21	Propan-1-ol	34	Polypropylene
9	BRN-SR2	22	Propan-2-ol	35	Nylon 6.6-101
10	LV1	23	Oleic acid	36	PMMA
11	IB3	24	Ethyl acetoacetate	37	Polycarbonaat
12	B200	25	Polyethylene glycol 200	38	Teflon
13	CB2-30%	26	Glycerol	39	Al2O3 99.7%

Table 16 – Materials given by [12]

1	Water	29	Liver 3	57	Skeleton - yellow marrow
2	Lung - blood filled	30	Muscle - skeletal 1	58	Head cranium
3	Lung - inflated	31	Muscle - skeletal 2	59	Head mandible
4	Adipose tissue 3	32	Muscle - skeletal 3	60	C4 excl. cartilage (male)
5	Adipose tissue 2	33	Pancreas	61	D6,L3 excl. cartilage (male)
6	Adipose tissue 1	34	Ovary	62	C4 incl. cartilage (male)
7	Mamary gland 1	35	Prostate	63	D6,L3 incl. cartilage (male)
8	Mamary gland 2	36	Testis	64	Vertebral column whole (male)
9	Mamary gland 3	37	Urine	65	Sternum
10	Breasts	38	Urinary bladder - empty	66	Clavicle, scapula
11	Brain - cerebrospinal fluid	39	Gallbladder - bile	67	Ribs 2nd, 6th (male)
12	Brain - grey matter	40	Spleen	68	Ribs 10th (male)
13	Brain - white matter	41	Thyroid	69	Humerus (total bone)
14	Brain and spinal cord	42	Trachea	70	Humerus spherical head
15	Adrenal gland	43	Aorta	71	Humerus cylindrical shaft
16	Misc. Glands	44	Blood - whole	72	Humerus whole specimen
17	Small intestine (wall)	45	Blood vessels	73	Pelvic innominate (male)
18	Stomach	46	Connective tissue	74	Pelvic innominate (female)
19	Gas.intest. tract - contents	47	Eyes	75	Pelvic sacrum (male)
20	Heart 1	48	Eye lens	76	Pelvic sacrum (female)
21	Heart 2	49	Lymph	77	Femur (total bone)
22	Heart 3	50	Skin 1	78	Femur sperical head
23	Heart - blood filled	51	Skin 2	79	Femur conical trochanter
24	Kidney 1	52	Skin 3	80	Femur cylindrical shaft
25	Kidney 2	53	Skeleton - cartilage	81	Femur whole specimen
26	Kidney 3	54	Skeleton - cortical bone	82	Lung - parenchyma
27	Liver 1	55	Skeleton - red marrow		
28	Liver 2	56	Skeleton - spongiosa		

Figure 17 – Tissues given by [13]

7.2 Hounsfield units

	Type of Material												
kV	1	2	3	4	5	6	7	8	9	10	11	12	13
30	1000	290	425	686	830	1033	1065	9685	754	1117	2325	2340	2947
40	1000	289	424	749	865	1025	1056	7798	831	1107	2024	2036	2535
50	1000	287	422	787	886	1017	1049	6634	877	1099	1833	1844	2273
60	1000	286	421	812	898	1012	1043	5893	906	1094	1709	1719	2104
70	1000	286	421	828	907	1008	1039	5389	926	1090	1624	1634	1988
80	1000	285	420	841	913	1005	1036	4996	942	1086	1558	1567	1897
90	1000	285	420	850	918	1003	1034	4706	953	1084	1509	1517	1829
100	1000	285	419	857	922	1001	1032	4493	961	1082	1473	1481	1780
110	1000	285	419	862	924	1000	1031	4329	968	1081	1445	1453	1741
120	1000	284	419	866	926	999	1030	4200	973	1079	1423	1431	1711
130	1000	284	419	870	928	998	1029	4096	977	1079	1405	1413	1687
140	1000	284	419	873	929	997	1028	4008	980	1078	1390	1398	1667
150	1000	284	419	875	931	997	1028	3935	983	1077	1378	1385	1649
kV	14	15	16	17	18	19	20	21	22	23	24	25	26
30	5005	7378	413	434	450	672	623	611	596	622	812	888	1074
40	4130	5969	476	500	518	705	669	666	649	694	860	944	1116
50	3575	5077	515	541	560	726	698	699	681	738	889	978	1141
60	3217	4501	539	566	586	739	715	720	702	766	907	1000	1157
70	2972	4108	555	583	603	747	727	734	716	784	919	1014	1167
80	2780	3799	568	597	617	754	737	745	726	799	929	1025	1176
90	2638	3571	578	607	627	759	744	753	734	810	936	1034	1182
100	2533	3403	585	614	635	763	749	759	740	818	941	1040	1186
110	2453	3274	590	619	641	766	753	763	745	824	945	1045	1190
120	2389	3172	594	624	645	768	756	767	748	828	948	1048	1193
130	2338	3089	598	627	649	770	758	770	751	832	951	1051	1195
140	2295	3021	600	630	652	771	760	772	753	836	953	1054	1197
150	2258	2962	603	633	655	772	762	775	755	838	955	1056	1198

(a) Materials 1 till 26

Table 18 – Hounsfield units determined with formula 8 for the materials[12]. In the first columns the tube voltage is given in kV.

	Type of tissue												
kV	1	2	3	4	5	6	7	8	9	10	11	12	13
30	1000	1071	265	692	737	783	806	905	1012	785	1042	1076	1038
40	1000	1064	263	755	793	832	854	934	1022	833	1034	1066	1038
50	1000	1059	262	793	827	861	882	951	1029	863	1028	1059	1037
60	1000	1056	262	817	849	880	900	962	1032	881	1025	1055	1037
70	1000	1054	261	834	863	893	912	969	1035	893	1023	1052	1036
80	1000	1053	261	846	874	902	922	975	1037	903	1021	1050	1036
90	1000	1051	260	855	883	910	929	979	1038	910	1020	1049	1036
100	1000	1050	260	862	889	915	934	982	1039	915	1019	1047	1036
110	1000	1050	260	868	893	919	938	985	1040	919	1018	1046	1035
120	1000	1049	260	872	897	922	941	987	1041	922	1017	1046	1035
130	1000	1049	260	875	900	925	944	988	1041	925	1017	1045	1035
140	1000	1048	260	878	902	927	946	989	1042	927	1016	1045	1035
150	1000	1048	260	880	905	929	948	990	1042	929	1016	1044	1035

(a) Tissues 1 till 13

kV	27	28	29	30	31	32	33	34	35	36	37	38	39
30	2101	1357	1708	2048	3012	1077	605	603	828	913	855	2457	8978
40	1804	1271	1539	1798	2534	1196	695	692	906	976	928	2316	7550
50	1620	1217	1433	1642	2234	1268	749	746	954	1013	972	2229	6672
60	1503	1183	1365	1541	2041	1313	783	780	984	1037	1000	2175	6114
70	1423	1159	1318	1472	1910	1344	806	803	1004	1053	1018	2137	5735
80	1361	1141	1282	1419	1807	1367	824	821	1020	1065	1033	2108	5440
90	1316	1127	1255	1379	1731	1385	838	834	1031	1074	1044	2087	5222
100	1282	1117	1235	1350	1675	1397	848	844	1040	1081	1052	2071	5061
110	1256	1109	1220	1328	1632	1407	855	851	1046	1086	1058	2059	4938
120	1236	1103	1208	1310	1599	1415	861	857	1052	1090	1062	2049	4841
130	1219	1098	1199	1296	1571	1421	866	862	1056	1093	1066	2041	4763
140	1205	1094	1191	1284	1548	1426	870	866	1059	1096	1069	2035	4697
150	1194	1091	1184	1273	1529	1431	873	869	1062	1099	1072	2029	4642

(b) Materials 27 till 39

Table 19 – Hounsfield units determined with equation 8 for the tissues [13]. In the first columns the tube voltage is given in kV.

kV	14	15	16	17	18	19	20	21	22	23	24	25	26
30	1059	950	1057	1014	1032	1024	1039	1054	1069	1089	1048	1060	1071
40	1053	970	1054	1017	1035	1023	1040	1051	1063	1080	1047	1056	1064
50	1050	981	1052	1019	1037	1023	1040	1050	1059	1074	1045	1053	1060
60	1047	989	1051	1020	1038	1022	1041	1048	1056	1071	1045	1051	1057
70	1045	994	1050	1021	1039	1022	1041	1048	1054	1068	1044	1050	1055
80	1044	998	1049	1021	1039	1021	1041	1047	1052	1066	1044	1049	1053
90	1043	1001	1048	1021	1039	1021	1041	1046	1051	1064	1043	1048	1052
100	1042	1003	1048	1022	1040	1021	1041	1046	1050	1063	1043	1047	1051
110	1042	1004	1047	1022	1040	1021	1041	1046	1050	1062	1043	1047	1050
120	1041	1005	1047	1022	1040	1020	1041	1045	1049	1061	1043	1046	1050
130	1041	1007	1047	1022	1040	1020	1041	1045	1049	1061	1042	1046	1049
140	1041	1007	1047	1022	1040	1020	1041	1045	1049	1060	1042	1046	1049
150	1040	1008	1047	1022	1040	1020	1041	1045	1048	1060	1042	1046	1049
kV	27	28	29	30	31	32	33	34	35	36	37	38	39
30	1059	1076	1091	1049	1060	1074	1018	1065	1038	1048	1085	1070	1038
40	1055	1070	1083	1047	1056	1066	1023	1060	1037	1045	1068	1061	1035
50	1052	1066	1078	1046	1053	1061	1025	1056	1036	1043	1057	1055	1033
60	1050	1063	1075	1045	1051	1057	1027	1054	1036	1041	1051	1051	1032
70	1049	1061	1073	1044	1049	1055	1028	1052	1036	1040	1046	1049	1031
80	1048	1060	1071	1043	1048	1053	1029	1051	1035	1040	1042	1047	1030
90	1047	1059	1070	1043	1047	1052	1029	1050	1035	1039	1040	1045	1030
100	1047	1058	1069	1043	1047	1051	1030	1050	1035	1039	1038	1044	1030
110	1046	1057	1068	1042	1046	1050	1030	1049	1035	1038	1036	1043	1029
120	1046	1057	1068	1042	1046	1049	1030	1049	1035	1038	1035	1043	1029
130	1046	1057	1067	1042	1046	1049	1030	1049	1035	1038	1034	1042	1029
140	1045	1056	1067	1042	1045	1048	1031	1048	1035	1038	1033	1042	1029
150	1045	1056	1066	1042	1045	1048	1031	1048	1034	1037	1033	1041	1029

(b) Tissues 14 till 39

kV	40	41	42	43	44	45	46	47	48	49	50	51	52
30	1079	1033	1088	1080	1093	1067	1085	1019	1009	1044	1032	1046	1067
40	1072	1035	1078	1070	1083	1061	1090	1019	1021	1038	1044	1055	1071
50	1068	1037	1072	1063	1077	1056	1093	1018	1028	1035	1052	1060	1073
60	1065	1038	1069	1059	1072	1053	1094	1018	1033	1033	1056	1063	1074
70	1063	1038	1066	1056	1069	1051	1095	1017	1036	1031	1059	1065	1075
80	1062	1039	1064	1054	1067	1049	1096	1017	1038	1030	1062	1067	1075
90	1060	1039	1062	1052	1065	1048	1097	1017	1040	1029	1064	1068	1076
100	1060	1039	1061	1051	1064	1047	1097	1017	1041	1029	1065	1069	1076
110	1059	1039	1060	1050	1063	1046	1097	1017	1042	1028	1066	1070	1076
120	1058	1039	1059	1049	1062	1046	1098	1017	1043	1028	1067	1070	1076
130	1058	1039	1059	1048	1061	1045	1098	1016	1044	1027	1067	1071	1076
140	1058	1040	1058	1048	1061	1045	1098	1016	1044	1027	1068	1071	1077
150	1057	1040	1058	1047	1060	1044	1098	1016	1045	1027	1068	1071	1077
kV	53	54	55	56	57	58	59	60	61	62	63	64	65
30	1241	7782	931	2262	743	5406	5903	3918	3277	3566	2976	3175	2623
40	1201	6285	956	1987	805	4437	4825	3280	2780	3007	2547	2703	2273
50	1176	5342	971	1813	843	3825	4145	2877	2466	2654	2276	2405	2051
60	1160	4734	980	1700	867	3432	3707	2618	2264	2427	2102	2213	1908
70	1149	4319	986	1622	883	3162	3407	2440	2125	2271	1982	2082	1810
80	1141	3994	991	1562	896	2952	3173	2301	2017	2150	1889	1979	1733
90	1135	3754	994	1517	905	2796	3000	2199	1937	2060	1820	1903	1676
100	1130	3577	997	1484	912	2681	2872	2123	1877	1993	1769	1847	1634
110	1126	3441	999	1459	917	2593	2774	2065	1832	1943	1730	1804	1602
120	1124	3334	1000	1439	921	2524	2697	2019	1796	1902	1699	1770	1577
130	1121	3246	1002	1423	925	2467	2634	1982	1767	1870	1674	1743	1556
140	1120	3174	1003	1409	928	2420	2582	1951	1743	1843	1653	1720	1539
150	1118	3113	1003	1398	930	2380	2537	1924	1722	1820	1635	1700	1525

(c) Tissues 40 till 65

kV	66	67	68	69	70	71	72	73	74	75	76	77	78
30	4353	3850	4694	4352	3380	4570	3796	3873	4238	2940	3681	4047	3380
40	3615	3227	3883	3615	2858	3784	3183	3244	3529	2519	3096	3378	2858
50	3149	2833	3372	3149	2528	3288	2796	2847	3081	2253	2726	2954	2528
60	2849	2580	3043	2849	2315	2969	2546	2591	2793	2081	2488	2682	2315
70	2644	2407	2817	2644	2169	2751	2375	2416	2595	1963	2325	2495	2169
80	2483	2271	2641	2483	2055	2580	2242	2279	2441	1871	2198	2349	2055
90	2364	2171	2511	2364	1971	2453	2143	2177	2327	1803	2104	2241	1971
100	2277	2097	2415	2277	1909	2360	2070	2103	2242	1753	2034	2162	1909
110	2210	2040	2341	2210	1861	2288	2014	2045	2178	1715	1981	2101	1861
120	2157	1995	2283	2156	1823	2232	1970	2000	2127	1684	1939	2052	1823
130	2113	1959	2236	2113	1793	2186	1934	1963	2086	1659	1905	2013	1793
140	2078	1928	2196	2078	1767	2148	1904	1933	2051	1639	1876	1981	1767
150	2047	1903	2163	2047	1746	2116	1879	1907	2022	1621	1852	1953	1746

kV	79	80	81	82
30	3577	6510	4094	1462
40	3012	5295	3415	1451
50	2655	4528	2986	1444
60	2425	4035	2709	1440
70	2268	3698	2520	1437
80	2144	3434	2372	1434
90	2053	3239	2263	1433
100	1986	3095	2182	1431
110	1935	2985	2120	1430
120	1894	2897	2071	1430
130	1861	2827	2032	1429
140	1833	2768	1999	1428
150	1810	2718	1971	1428

(d) Tissues 66 till 82

	lung - inflated			Adiopose tissue 2			Liver 2		
kV	H	H+10	H-10	H	H+10	H-10	H	H+10	H-10
30	265	275	255	737	747	727	1076	1086	1066
60	262	272	252	849	859	839	1063	1073	1053
90	260	270	250	883	893	873	1059	1069	1049
100	260	270	250	889	899	879	1058	1068	1048
150	260	270	250	905	915	895	1056	1066	1046
	Muscle skeletal 2			Skeleton - cortical bone			Humerus (total bone)		
kV	H	H+10	H-10	H	H+10	H-10	H	H+10	H-10
30	1060	1070	1050	7782	7792	7772	4352	4362	4342
60	1051	1061	1041	4734	4744	4724	2849	2859	2839
90	1047	1057	1037	3754	3764	3744	2364	2374	2354
100	1047	1057	1037	3577	3587	3567	2277	2287	2267
150	1045	1055	1035	3113	3123	3103	2047	2057	2037

Table 20 – Introduced noise on the Hounsfield units for six different tissues

7.3 Relative electron densities estimated with reference materials AlMgSi1 and CB2-30%

To explain why the $\mathrm{RED}_{\mathrm{calc}}$ is estimated larger for the reference material like AlMgSi1 and smaller for the reference material for CB2-30%, equation 13 is used. This equation can be rewritten in a way such that the difference between H_1 and H_2 is apparent. This can be seen in equation 23.

$$\mathrm{RED} = \frac{H_2}{1000} + a\left(\frac{H_1 - H_2}{1000}\right) \tag{23}$$

The difference of ΔH for AlMgSi1 is larger than the difference for CB2-30% this can be explained with the following derivation:

$$H_1 - H_2 = 1000\left(\frac{\mu_{x,1}}{\mu_{H_2O,1}} - \frac{\mu_{x,2}}{\mu_{H_2O,2}}\right) \tag{24}$$

Since ΔH is negative for both reference materials, the attenuation coefficients should obey the following equation:

$$\frac{\mu_{x,1}}{\mu_{H_2O,1}} < \frac{\mu_{x,2}}{\mu_{H_2O,2}} \tag{25}$$

Which can rewritten as:

$$\frac{\mu_{H_2O,2}}{\mu_{H_2O,1}} < \frac{\mu_{x,2}}{\mu_{x,1}} \tag{26}$$

This means that the attenuation coefficients both drop faster relative to water with an increasing tube voltage. Moreover, the drop of the attenuation coefficient of AlMgSi1 is even larger than the drop of CB2-30%, resulting in a larger ΔH.

The influence of the different a values on the relative electron density depend on the sign of $H_1 - H_2$. Which is the cause of the different accuracy's of the relative electron density obtained with AlMgSi1 and the relative electron densities obtained with CB2-30%.
If $H_1 < H_2$ the second term of equation 23 will become negative. A larger a value (reference material CB2-30%) will amplify this effect. Such that the calculated relative electron density obtained with CB2-30% will turn out smaller.

If $H_1 > H_2$ the second term of equation 23 will become positive. A larger a value (reference material CB2-30%) will amplify this effect. Such that the calculated relative electron density obtained with CB2-30% will turn out larger. These both effects can be seen in figure 7.

7.4 Determination of n

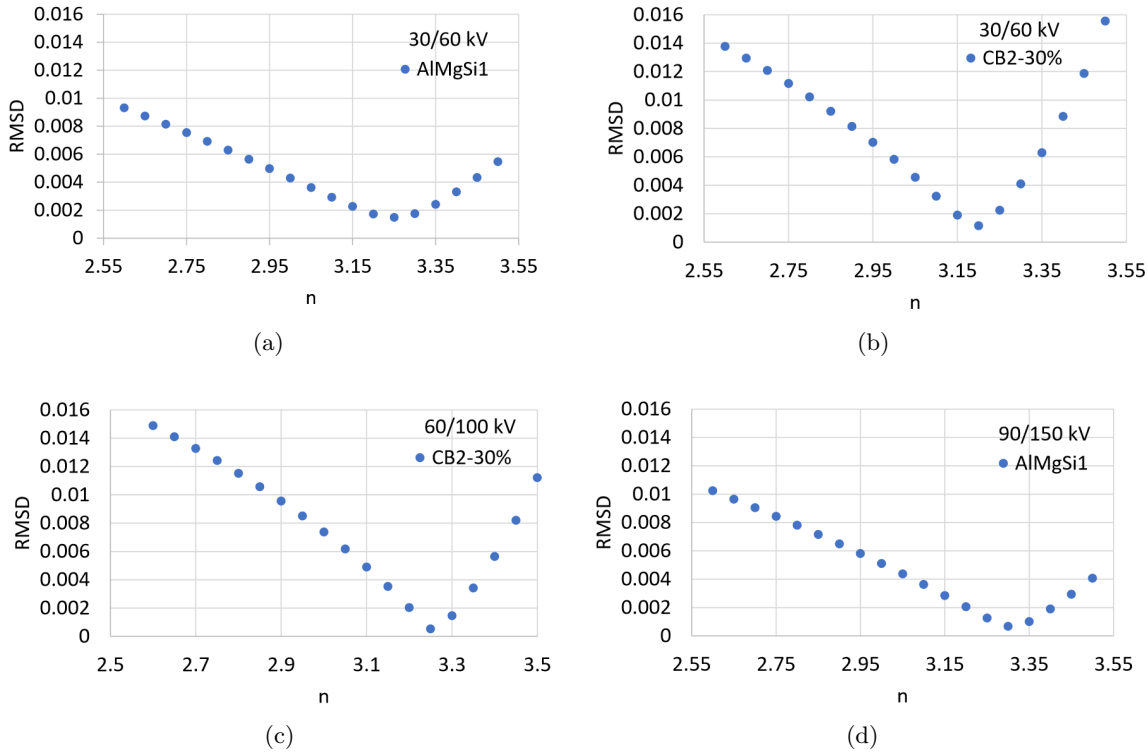

Figure 21 – The RMSD obtained with equation 22 as a function of n